Turbofan Aft-Radiated Broadband Acoustic Flight Effects

Ian A. Clark*, Eric H. Nesbitt†, Russell H. Thomas‡, and Yueping Guo‡
NASA Langley Research Center, Hampton, VA 23681 USA

This paper presents the status and ongoing development of a new model for the prediction of aft-radiated turbofan broadband noise. The proposed model is developed using data from two full-scale flight tests, the Boeing Quiet Technology Demonstrator 2 (QTD2) and the NASA/Boeing Propulsion Airframe Aeroacoustics and Aircraft System Noise (PAA&ASN) flight tests. The proposed model accounts for an observed coupling between directivity and fan relative tip Mach number. Additional features such as improved spectral and directivity characteristics are discussed. Significant improvements over prior methods implemented in the NASA Aircraft Noise Prediction Program are demonstrated, and predicted deltas to measured levels are reduced from +10/-20 dB to ±3 dB or better at the most relevant frequencies. This is expected to greatly improve the ability of NASA to predict the noise of both current and future aircraft concepts.

I. Introduction

Projected growth of the aviation sector highlights the need for significant reduction in environmental impact to ensure a sustainable future for the globe and for local communities around airports while meeting market demands for improved payload, speed, and range performance. The goal of the NASA Advanced Air Transport Technology (AATT) Project is to explore and develop technologies and concepts for safe, economical, energy-efficient, and quiet fixed-wing subsonic transports [1]. To inform technology development planning and decision-making, the AATT Project is continually improving the quality of system noise assessments of current and prospective aircraft. Full-scale flight data are a critical means of improving and validating system noise assessment tools, including the NASA Aircraft NOise Prediction Program (ANOPP).

Fan source noise, the performance of engine acoustic liners, and Propulsion Airframe Aeroacoustics (PAA) effects associated with fan noise are key elements of system noise, even for aircraft concepts that feature significant engine noise shielding. June et al. [2] found that a strong majority of uncertainty present in the system noise prediction of a hybrid-wing body (HWB) aircraft could be attributed to the prediction of fan source levels, engine acoustic liner performance, fan PAA effects, and Krueger flap noise. NASA has funded research on Transonic Truss-Braced Wing (TTBW) configurations both internally and externally [3] since 2010, leading to the planned test of the X-66A demonstrator in coming years. The most recent acoustic assessment of the TTBW concept [4] shows fan noise, liner, and PAA effects to be critical to the overall noise and key targets for noise reduction technology. In spite of the demonstrated importance of fan noise, liner effects, and PAA effects, limited in-flight acoustic data are available to rigorously evaluate the modeling of these effects.

To address this limitation, the Propulsion Airframe Aeroacoustics and Aircraft System Noise (PAA&ASN) flight test was performed in August 2020 in collaboration with The Boeing Company as part of the ecoDemonstrator 2020 program. The test was carefully designed for high signal-to-noise ratio and repeatability, yielding a complete dataset with which to evaluate many of the models that comprise ANOPP, including those for fan noise and liner effects. An overview of the full test campaign is presented by Thomas et al. [5] and Czech et al. [6]. Clark et al. [7] performed a first analysis of the measurements focused on fan noise and liner effects and found significant discrepancies between the measured noise and noise predicted using the method of Krejsa and Stone [8], particularly in the aft arc. The aft directivity was found to vary significantly with throttle setting, a feature that is not present in the prediction model.

The current work extends the work of Clark et al. [7] by improving the analysis of fan noise data. In particular, the fan broadband noise is the focus of the current work, while fan tones are treated separately in a companion publication by Nesbitt et al. [9]. The previous analyses and conclusions [7] offered several opportunities for improvement. First, the fan noise spectra were not separated into tonal and broadband components. These components have different physical mechanisms responsible for their generation, and as a result, exhibit different characteristics with respect to directivity,

*Research Aerospace Engineer, Aeroacoustics Branch, AIAA Senior Member, ian.a.clark@nasa.gov.
†Senior Research Engineer, Aeroacoustics Branch, AIAA Senior Member.
‡Senior Research Engineer, Aeroacoustics Branch, AIAA Associate Fellow.

throttle setting, etc. Second, while fan noise was extracted from total flyover noise using a process that involved ANOPP predictions and post-processing additional flight test configuration data, the resulting fan noise spectra were limited in frequency range due to masking by uncertainties in the subtracted components. Third, the fan noise was not decomposed into inlet- and aft-radiated components, which again have different physics governing their generation and propagation and exhibit their own scaling characteristics. The present work seeks to overcome these limitations through more advanced processing and additional steps to better isolate fan noise from flyover data and to separate that fan noise into constituent components. In addition, data from the Boeing Quiet Technology Demonstrator 2 (QTD2) test [10] conducted in 2005 are utilized in this study to broaden the database and consider the effects of two different engines.

To make progress toward improved system-level predictions, of which fan noise plays a key part, the functional forms of current fan noise models will be investigated and modified in an attempt to find better correlating parameters that can more accurately predict fan noise across a range of conditions and fan designs. Improvements will be made to the throttle setting and directivity characteristics of the fan prediction which were shown to be sources of significant discrepancy in Clark et al. [7]. Spectral shape characteristics will also be addressed. Finally, the reformulated prediction will be verified via direct comparison to the PAA&ASN 787 flight test data to confirm and characterize the potential improvements of the proposed framework. Aft-radiated fan broadband noise will be the focus of this paper, and this framework will be expanded for inlet-radiated fan broadband noise in future work.

II. Flight Test Setup

The NASA PAA&ASN flight test was conducted in collaboration with The Boeing Company as part of their 2020 ecoDemonstrator program. Extensive acoustic measurements were made on a newly manufactured Boeing 787-10 Etihad Airways airliner with GEnx-1B engines. For the test conditions considered in this paper, the port engine was set at a target N1C (corrected fan shaft rotation speed), while the starboard engine was kept at flight idle. Flight data recorders on board the aircraft enabled highly accurate, time-resolved aircraft state telemetry. The test site was a privately owned airfield near Glasgow, MT with no other air traffic in the vicinity. Ground-based instrumentation included eight community microphone arrays with 42 ground-board microphones in total (see Fig. 1). This paper focuses primarily on the centerline microphone array, which contained eight microphones for high-quality averaging. Further details of the PAA&ASN flight test setup are provided by Czech et al. [6].

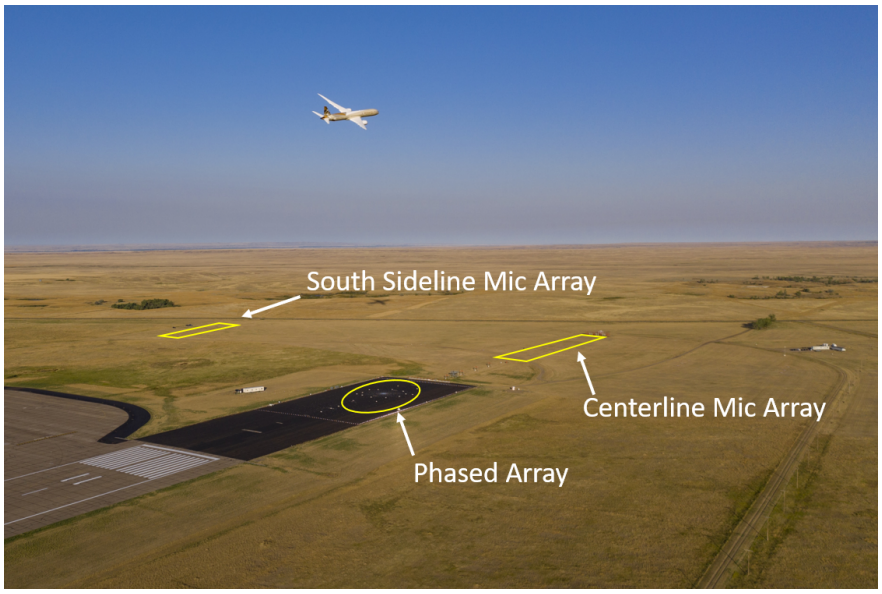

Fig. 1 Drone photograph of test aircraft flying over acoustic instrumentation. Array locations highlighted in yellow for clarity. Not all arrays are shown/highlighted. Photo credit: The Boeing Company.

A variety of aircraft configurations were measured throughout the five test days of the NASA PAA&ASN flight test. In addition to the production (unmodified) configuration, a hardwalled configuration was tested, in which aluminum tape was used to cover the aft bypass duct liner, thereby removing the acoustic effect of the liner. In each configuration,

a series of flyovers were performed at intervals of throttle setting. These conditions are the focus of this paper.

In addition to the primary dataset from the PAA&ASN flight test, data from the QTD2 flight test, conducted on a Boeing 777-300ER airplane equipped with GE90-115B engines, will also be used to supplement the analysis of fan noise. This flight test was conducted at the same test site as the PAA&ASN flight test, with a similar setup and layout of ground-based microphone instrumentation. Further details of the QTD2 flight test are provided by Herkes et al. [10].

III. Data Processing

In contrast to the analysis of Clark et al. [7], which began with one-third octave band acoustic data, this paper begins analysis with narrowband acoustic data. Standard data processing as developed for noise certification testing was used to generate narrowband spectra from the time-series data and to correct for atmospheric conditions, normalize to a standard flight path, and ensemble average. Time-dependent narrowband spectra were delivered with a polar angle resolution of two degrees; each spectrum was generated from 0.16-second segments of pressure time history with 50% overlap and ensemble averaged over the microphones in the array.

For this study, the tone-accurate narrowband spectra were first processed to remove the Doppler frequency shift using the precise Mach number recorded during each individual flyover and the reported emission angle for each spectrum. The spectra were then backpropagated to convert to equivalent 1-ft lossless spectra, removing the effects of spherical spreading and atmospheric absorption using the method described in ANSI S1.26-1995. Broadband noise was then extracted from the spectra using a median filter stencil method [11], followed by the minimum broadband algorithm described by Nesbitt et al. [12]. As described in the companion paper on turbofan tones [9], this combined algorithm yields a high-quality estimate of the broadband noise without including the broad "hay-stack" tones that are otherwise included by the median filter alone. Finally, the narrowband spectra were integrated to one-third octave band spectra and calibrated to the 0.5-second integration one-third octave data.

The resulting broadband noise represented the total broadband noise measured from all sources on the aircraft, including airframe noise and engine noise sources other than fan noise. In order to isolate fan noise, a component build-up approach was used to model the spectral shape of all sources to be removed, including jet, jet-flap interaction, airframe, and combustor (core) noise. Independent models were built for all throttle settings and emission angles. The resulting spectra were then fit to the low-frequency region of the measured data, where fan noise was expected to be a non-dominant contributor to the total levels. This process is illustrated notionally in Fig. 2(a). The fitted spectra were then subtracted from the total measured levels on a pressure-squared basis, with the result representing fan noise, as illustrated in Fig. 2(b). The subtraction was performed iteratively from high frequency to low frequency, and at each frequency the difference between the measured data and fitted sum was computed. As the difference approached some specified small value, the spectral subtraction was terminated and a constant slope was applied to reconstruct the low-frequency spectral shape as indicated by the gray region in Fig. 2(b).

Only hardwalled aft duct configurations from the PAA&ASN 787 flight test were considered for this work, but the QTD2 dataset only included production (lined) aft duct results. To remove the effects of the liner and approximate an equivalent hardwalled configuration for the QTD2 dataset, the liner attenuation prediction method of Kontos et al. [13] was used to estimate the liner performance and shift the measured levels appropriately. In addition, propulsion airframe aeroacoustic (PAA) effects were estimated from data acquired in the Boeing Low Speed Aeroacoustic Facility (LSAF) [14] and were removed from the extracted fan broadband levels. As mentioned above, the focus of the present work is aft-radiated broadband noise. Rather than attempt to explicitly separate inlet- and aft-radiated contributions at all emission angles, this work will simply focus on emission angles from 80 to 150 deg relative to the inlet axis. Comparisons between noise levels measured for the hardwalled and production aft duct configurations revealed that aft-radiated contributions to total levels are dominant at these angles.

IV. Fan Noise Prediction

In contrast to the prior work of Clark et al. [7], the individual subcomponents of fan noise as predicted by the method of Krejsa and Stone [8] will not be combined into total fan noise. The predicted aft-radiated broadband noise will be compared directly with the corresponding extracted fan noise subcomponent as described in the previous section. The predictions were made using Boeing-provided information on the aircraft engine cycle and flight conditions for each individual flyover and input to the method of Krejsa and Stone [8].

The method of Krejsa and Stone [8] can be described as a recalibration of the prior method of Heidmann [15]. There have been other recalibrations published, including the method of Hough and Weir for small engines [16], and the

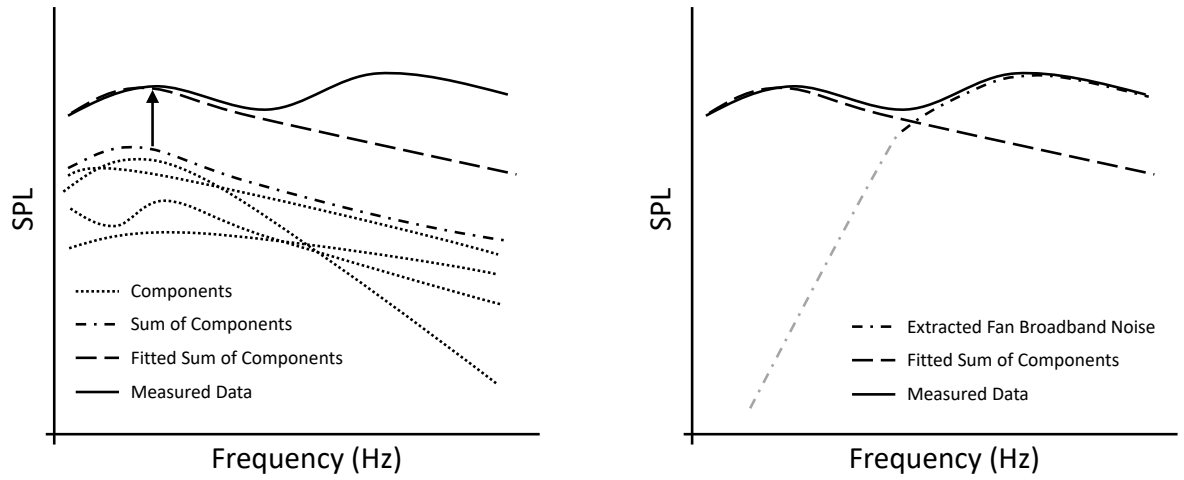

(a) Component Buildup and Fit **(b) Spectral Subtraction**

Fig. 2 Notional illustration of process to isolate fan broadband noise from total measured broadband noise.

method of Kontos et al. [17] for large engines. In most cases, the functional forms have remained the same. However, the method of Krejsa is unique in several ways, as seen in Eq. 1 for the aft broadband noise in particular.

$$SPL = 10\log_{10}(\dot{m}/\dot{m}_0) + 40\log_{10}(\Delta T/\Delta T_0) + 34.0 - 17.0(M_r - 0.65) - 5\log_{10}(RSS/300) + f_1(\theta) + f_2(f) \quad (1)$$

First, while the three other methods correlate sound pressure level to the second power of the total temperature rise across the fan (ΔT), Krejsa puts a fourth-power dependence on this parameter. Second, while other methods express a logarithmic dependence between SPL in decibels and tip relative Mach number (M_r), which is anticipated by the physics of aerodynamic noise generation, Krejsa expresses a linear relationship between these two quantities.

Considering the Krejsa method more generally, other characteristics are interesting to note. The correlating parameters include mass flow rate ($\dot{m}$), temperature rise across the fan, and tip Mach number. These three parameters are not independent for a given fan, but rather rise and fall together in response to throttle setting. In the model, sound pressure level increases with mass flow rate and temperature rise, but decreases with tip Mach number. While each parameter independently would be expected to be positively correlated with SPL, the inclusion of all three parameters required a negative correlation on tip Mach number to best collapse the source data. This is analogous to overfitting and could lead to a less generalized model with degraded performance outside of the training dataset. Other frameworks will be considered in this work to yield a more stable model.

V. Model Development

A. Spectral Fitting

Beginning from the fan noise spectra obtained from the process outlined in Section III, the first step to fitting the data to a model framework was fitting a spectral shape to the data. For this, the general functional form of the spectral shape function used by the Heidmann [15] method and its derivatives was used, as shown in Eq. 2.

$$f(\theta) = 10\log_{10}\exp\left\{-0.5\left[\frac{\ln(\eta/C)}{\ln(\sigma)}\right]^2\right\} \quad (2)$$

Here, η is the frequency normalized by the blade passage frequency (since the data are de-Dopplerized), C is a constant that places the peak of the spectra at C times the blade passage frequency, and σ is a constant set to 2.2 as in the Krejsa method. For a given dataset (PAA&ASN 787 or QTD2), the value of C was chosen to give good agreement to the spectral shape at overhead angles and was kept constant for all angles and thrust settings. For each individual angle and thrust setting, the spectral shape was shifted in level to minimize the root-mean-square error between the

modeled spectrum and the measured spectrum in a frequency range from 1-5 kHz, where fan noise was observed to peak in the data. The main objective of this procedure, which is notionally illustrated in Fig. 3(a) was to yield a smoothly-varying estimate of the peak level as it changes with angle and thrust setting. As illustrated in the figure, due

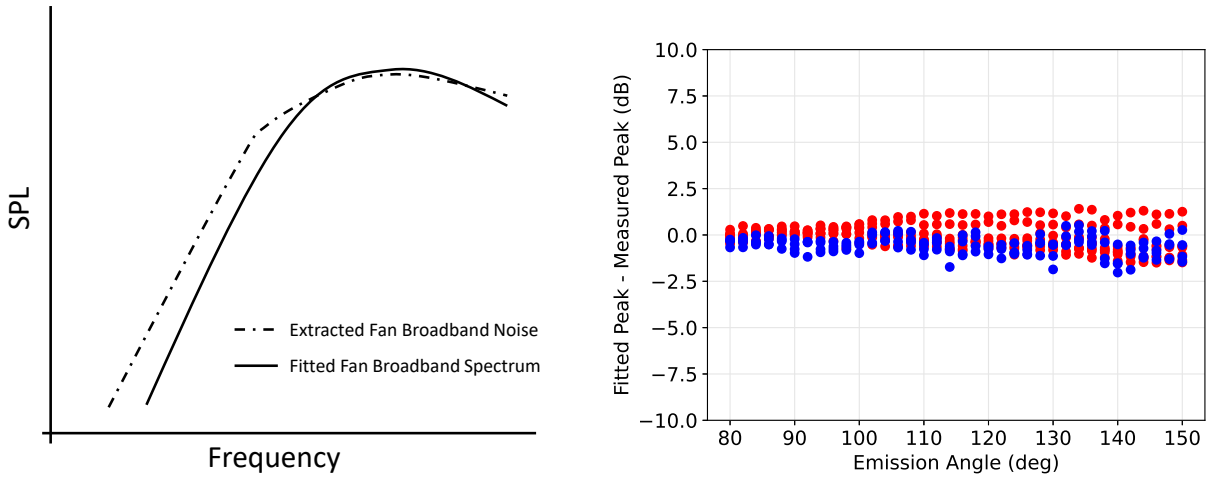

(a) Spectral Fitting Process **(b) Spectral Fit Quality**

Fig. 3 Notional ilustration of spectral fitting process, with differences between peaks as extracted by fitting spectral shape function to data and as measured. PAA&ASN 787 data are shown in red, QTD2 data are shown in blue.

to the variation between the modeled spectral shape and the true shape of the data, the modeled and measured peak levels do not generally match. The differences between the fitted peak and the absolute measured peak at all angles and throttle settings for the two datasets is shown in Fig. 3(b).

As can be seen in the figure, generally good agreement is achieved with this method, with the extracted fitted peak agreeing with the absolute measured peak to within ±2 dB in most cases. More scatter is observed at far aft angles, where data quality decreases and the spectral characteristics of the measured data do not follow trends as clearly as observed nearer the overhead angles.

B. Power Setting Normalization

As discussed in Section IV, the Krejsa model has some unique characteristics such as a strong dependence on fan temperature rise and a negative linear dependence on fan tip relative Mach number. As discussed in Clark et al. [7], the model shows disagreement with the PAA&ASN 787 flight test data at low throttle settings and aft angles, which indicates that the throttle setting dependence could be improved. The prior work also showed a change in directivity with throttle setting.

For a given fan (constant design tip Mach number, rotor-stator spacing, etc.), the Krejsa dependence on throttle setting for aft-radiated broadband noise is given in Eq. 3.

$$SPL \propto 10\log_{10}\dot{m} + 40\log_{10}\Delta T - 17.0M_r \tag{3}$$

Here, $\dot{m}$ is mass flow rate through the fan, ΔT is total temperature rise across the fan, and M_r is tip relative Mach number. The mass flow parameter is also useful for correlating noise levels across different fans of different sizes, but the temperature rise and tip relative Mach number terms contradict. After testing several formulations, it was found that the best data collapse for the 787 flight test data could be achieved by neglecting the temperature rise term and correlating solely on the logarithm of relative tip Mach number, as given in Eq. 4, where A is a constant yielding the best fit, to be found via regression.

$$SPL \propto 10\log_{10}\dot{m} + A\log_{10}M_r \tag{4}$$

The difference in the two approaches can be seen in Fig. 4, where the collapse of the peaks for all throttle settings and emission angles is shown. In Fig. 4(b), the coefficient A in Eq. 4 is optimized for best fit in the near-overhead angular range, between approximately 80 and 110 degrees. The normalized levels are shown relative to one particular thrust setting, separately for the 787 and QTD2 datasets, such that ideal model performance would place all datapoints at 0 dB for all emission angles.

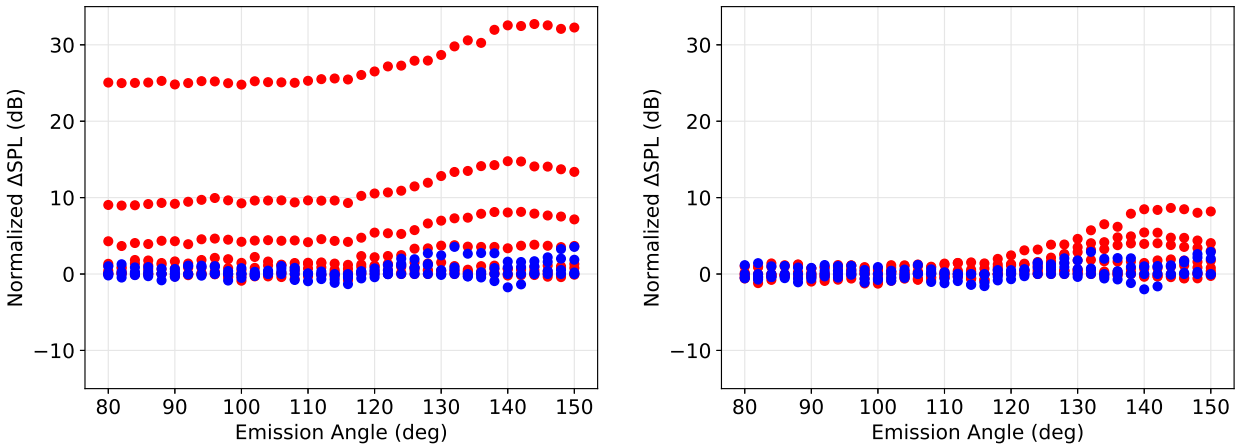

(a) Krejsa Normalization **(b) Overhead-Fitted Normalization**

Fig. 4 Quality of normalization based on relations of Krejsa vs the proposed formulation fitted to overhead angles. PAA&ASN 787 data are shown in red, QTD2 data are shown in blue.

As can be seen in the figure, the proposed formulation and fit greatly improve the data collapse from a 25 dB spread to about a 3 dB spread at near-overhead angles, indicating a more accurate relationship between operating condition and sound pressure level. However, the collapse is still not satisfactory at aft angles, and choosing a different value of A to improve the fit at aft angles would necessarily degrade the performance in the overhead region. It is clear that there is no single value of A that would yield accurate prediction of levels across all emission angles. Therefore, as a next step, the constant A is replaced with a function of emission angle $\beta(\theta)$. To understand the characteristics of $\beta(\theta)$, the value of β is found at each emission angle individually by finding the best collapse of the 787 data. As seen in Fig. 5, a blending function based on the error function (Eq. 5) is easily fit to the results, and can be used to normalize SPL as in Eq. 6.

$$\beta(\theta) = A + B\left(\mathrm{erf}\left(\frac{\theta - C}{D}\right)\right) \tag{5}$$

$$SPL \propto 10\log_{10}\dot{m} + \beta(\theta)\log_{10} M_r \tag{6}$$

In Eq. 5, the constants A, B, C, and D define the shape and position of the blending function. Normalizing on the proposed relation in Eq. 6 yields Fig. 5(b), where good data collapse is observed at all angles. This purely empirical approach to model development does not yield a physical understanding of the broadband noise behavior; however, there are several notional explanations. Several sources of fan broadband noise exist, including the interaction of the inlet boundary layer with the rotor, rotor self-noise, and turbulence from the rotor wakes impinging on the stators. While these have similar physical mechanisms (scattering of convected turbulence), one possible explanation for the observed behavior is that two hypotheses are simultaneously true. First, the physical sources of fan broadband noise scale differently on rotor tip Mach number. Second, the physical sources generate noise with different far-field directivities. Together, this would indicate that some physical sources scale on a certain tip Mach number and propagate primarily to overhead directions, while other sources scale on a different tip Mach number and propagate primarily aft. There is some physical grounding in the first statement - rotor self-noise scales differently than the rotor leading-edge noise produced by interaction with the inlet boundary layer, for example. However, there is less evidence available to assess the second hypothesis regarding directivity, especially since broadband noise is less organized into specific duct modes as would be the case with tones. This hypothesis requires additional research with more detailed information than is available for this study.

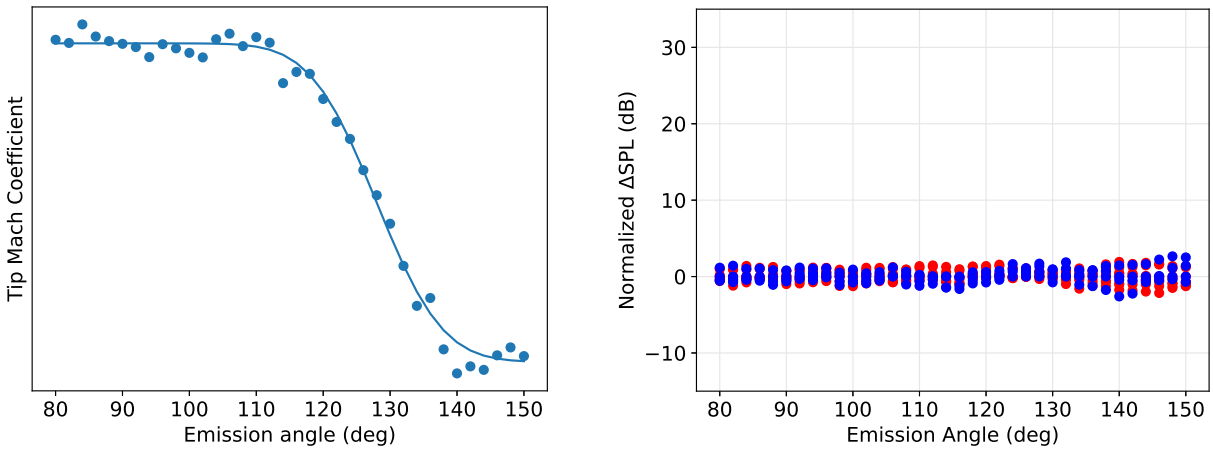

(a) Error Function Fit **(b) Full Normalization**

Fig. 5 Fitting of blending function for coefficient of tip relative Mach number dependence, and quality of normalization based on the fully-defined proposed formulation. PAA&ASN 787 data are shown in red, QTD2 data are shown in blue.

C. Directivity

The throttle-dependent directivity characteristics have been covered in the previous section, which now makes the choice of a general function for directivity more straightforward. By scaling the spectral peak levels using the function given in Eq. 6 above, a clear directivity function was revealed once the data were normalized to the peak emission angle, at least for a given data set. While not shown here, some minor but significant differences were observed in the directivity characteristics between the PAA&ASN 787 flight test and the QTD2 flight test, as might be expected for different engines. To move forward with a generalized model, a directivity function was chosen that was best fit to both datasets simultaneously, and it remains for future work to develop a more complete directivity model that accounts for specific characteristics of a given engine (geometry, etc.).

D. General Prediction

With the individual fan-specific frameworks for spectral shape, throttle dependence, and directivity established, a general function for aft broadband noise prediction can be expressed as in Eq. 7.

$$\begin{aligned} SPL = {} & a_0 + a_1 \log_{10}(1 - M_\infty cos(\theta)) + a_2 \log_{10} A_{eff} \\ & + a_3 \log_{10} M_r + a_4 \left(\text{erf}\left(\frac{\theta - C}{D} \right) \right) \log_{10} M_r \\ & + a_5 \log_{10} M_{des} + a_6 \log_{10} RSS + f_1(\theta) + f_2(f) \end{aligned} \tag{7}$$

Here, a_0 is a constant, the a_1 term corresponds to convective amplification, the a_2 term corresponds to the bypass nozzle effective area, the a_3 and a_4 terms correspond to the tip relative Mach number dependence of the same general form as Eq. 5, the a_5 term corresponds to the design relative tip Mach number at the Aerodynamic Design Point (ADP), and the a_6 term corresponds to the rotor stator spacing (RSS). Finally, $f_1(\theta)$ is the general directivity function and $f_2(f)$ is the spectral shape as a function of frequency.

It is noted here that the effective area A_{eff} has replaced the mass flow rate $\dot{m}$ to correlate over engine size. With only two datasets, it is impossible to say purely from the data which parameter might be better suited to a general model for any arbitrary engine. However, it is expected that the effective area embodies characteristics that are key to fan noise, including bypass nozzle performance, in addition to simple geometric scaling. In total, three design variables are present in Eq. 7, namely effective area, design tip Mach number at ADP, and rotor-stator spacing, but only two datasets and engine designs are available for fitting. As a result, two coefficients (a_i) are chosen manually based on prior convention, and one is left for the fitting routine to best collapse the two datasets.

To choose the remaining coefficients, the differential evolution optimization method of Storn and Price [18] was used as a multivariable regression solver to fit the spectral peak levels to the measured spectral peaks, which is given by removing the term $f_2(f)$ from Eq. 7. The final coefficient solutions converged to values that were well within the specified bounds, and the r^2 value was approximately 0.98 indicating an excellent fit. The resulting model performance is shown in Fig. 6, where datapoints for all datasets, throttle settings, and directivity angles between 80 and 150 deg are shown, and the diagonal line represents equal predicted and measured levels.

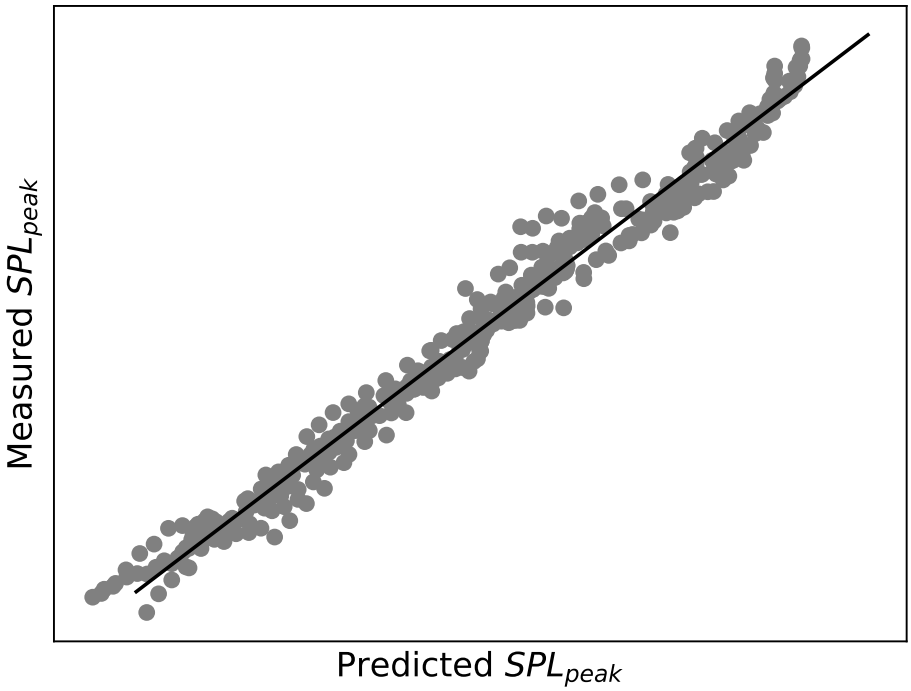

Fig. 6 Quality of multiple linear regression analysis to fit the model framework to the measured data.

VI. Comparison to Data

In order to verify the model resulting from the above procedure, comparisons similar to those shown in Clark et al. [7] are now shown here comparing both the Krejsa model and the proposed prediction model. It is emphasized that this is a model verification, demonstrating the performance against the training data in a clear way. Model validation requires an additional, independent dataset that was not included in the model fitting procedure, and this remains for future work.

Spectral comparisons are first shown for two representative emission angles, one near overhead (Fig. 7) and one at an aft emission angle (Fig. 8). The first and most obvious improvement with the proposed prediction is the reduction in absolute differences for the lowest thrust cases, but the agreement with mid to high thrust is improved as well. Generally, agreement between predicted and measured levels has been improved from approximately +10/-20 dB for the Krejsa method to ±3 dB or better for the proposed model in the frequency range surrounding the spectral peak. In addition, the negative slope in the curves comparing the Krejsa prediction to data indicate a mismatch in spectral shape between prediction and measured data. With the improved spectral fit as discussed in Section V.A, the proposed prediction shows a more constant trend with frequency. More discrepancy between the proposed prediction and measured data is observed at lower frequencies; however these values represent levels farther from the spectral peak, and where the uncertainty is greater in the low-frequency component subtraction process used to isolate fan noise.

To show additional trends as presented in Clark et al. [7], Figs. 9 and 10 show additional normalized comparisons between prediction and measurement. Note that some differences are observed between the Krejsa comparisons presented here and those presented previously because the prior work made no attempt to separate broadband and tone levels.

To isolate the directivity trends, for each operating condition, the peak spectral level at each emission angle was

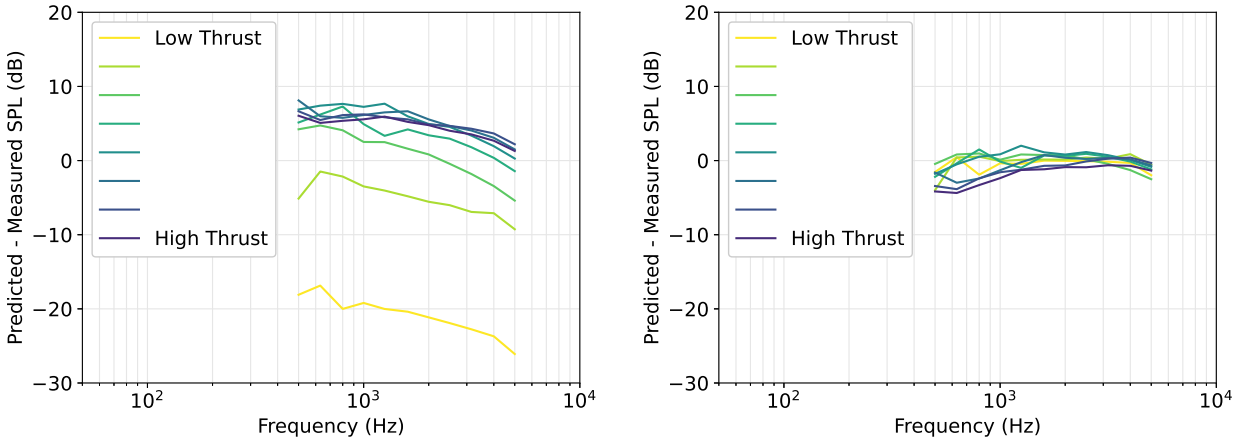

(a) Krejsa Prediction **(b) Proposed Prediction**

Fig. 7 Differences (Prediction−Data) in fan broadband one-third octave band SPL predicted using Krejsa and the proposed formulation at a near-overhead angle.

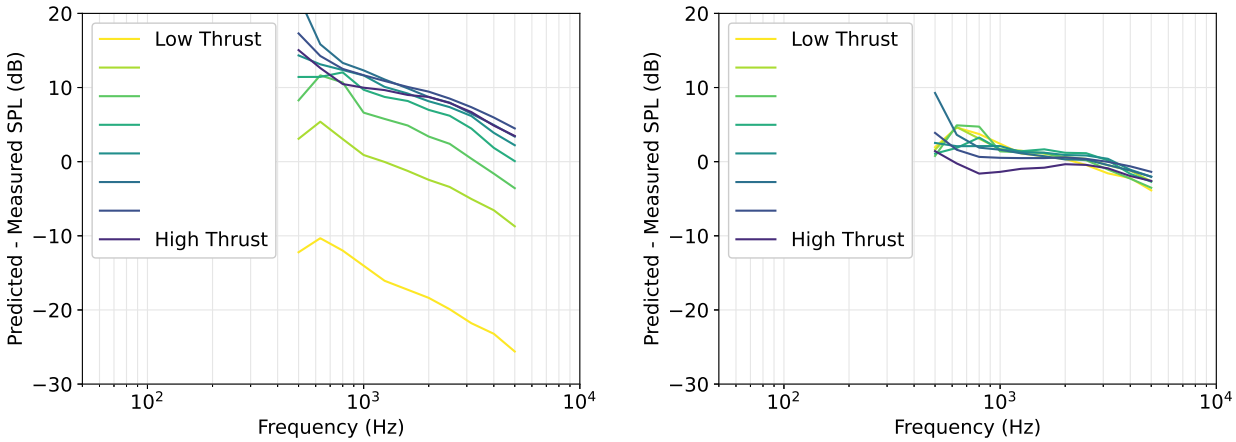

(a) Krejsa Prediction **(b) Proposed Prediction**

Fig. 8 Differences (Prediction−Data) in fan broadband one-third octave band SPL predicted using Krejsa and the proposed formulation at an aft angle.

normalized relative to the peak at 90 degrees (overhead) emission angle. Figure 9 shows the difference between the predicted and measured normalized peaks, where the ideal prediction of directivity would lie on the 0 dB line. As observed in the prior work, not only is there a mismatch in directivity pattern for all thrust settings in the Krejsa model, there is also a dependence on thrust setting at aft angles. The maximum absolute difference in relative directivity approaches 9 dB, with a nearly 6 dB spread over thrust settings at aft angles. The proposed prediction framework, which couples directivity with tip Mach number, not only shows better overall agreement at all emission angles by limiting the maximum absolute difference in relative directivity to 2 dB, but also largely removes the throttle setting dependence on directivity at aft angles.

To isolate the effect of throttle setting, at each emission angle, the peak spectral levels are normalized to the peak level at the highest throttle setting separately for the predicted and measured data. Figure 10 shows the difference between the normalized measured peaks and the normalized predicted peaks at each throttle setting, which demonstrates the difference between the predicted and measured correlation of noise levels with thrust. The ideal prediction of the noise level response to thrust setting would lie on the 0 dB line. Again, as observed in prior work, the extreme sensitivity of the Krejsa prediction at low thrust settings is demonstrated here, while the proposed prediction framework is stable

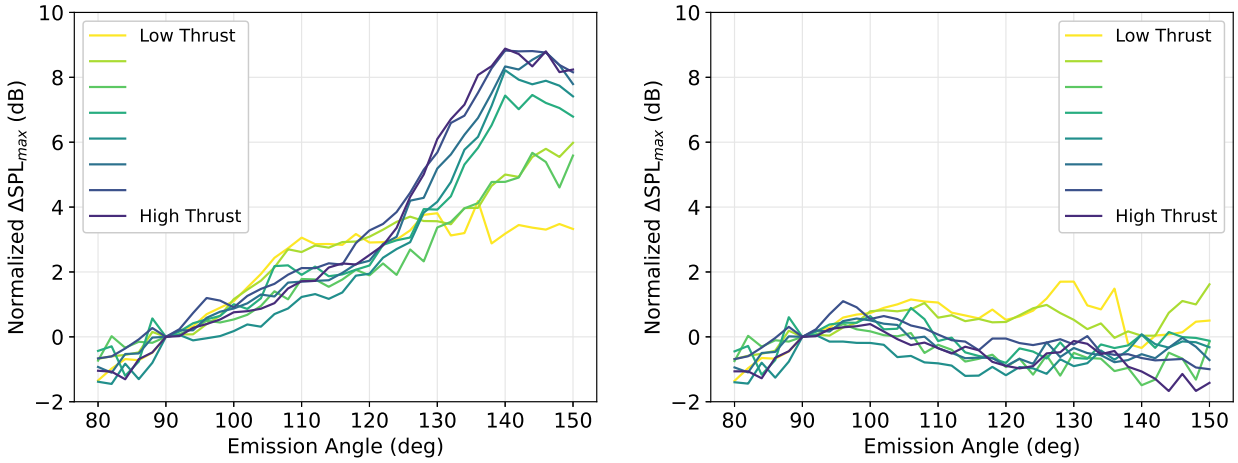

(a) Krejsa Prediction **(b) Proposed Prediction**

Fig. 9 Normalized differences (Prediction−Data) in directivity trends of aft fan broadband noise.

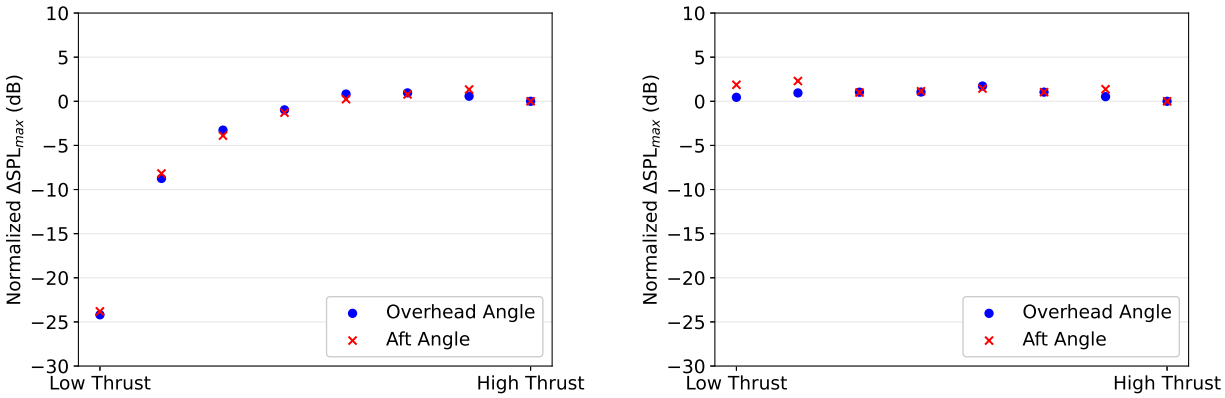

(a) Krejsa Prediction **(b) Proposed Prediction**

Fig. 10 Normalized differences (Prediction−Data) in thrust setting trends of aft fan broadband noise.

even at low thrust. The proposed prediction suggests a slight overprediction at moderate thrust levels, but this is an artifact of the normalization process. As Figs. 7 and 8 show, the highest thrust setting is slightly underpredicted, and because this case is the basis for the normalization, the other thrust settings are shifted above the 0 dB line in Fig. 10(b).

VII. Conclusions and Future Work

A new system-level noise prediction model for aft-radiated turbofan broadband noise has been formulated using two full-scale flight test datasets. The general performance of the new formulation has been shown to greatly improve prediction characteristics for a range of fan operating conditions, emission angles, and frequencies. Prediction deltas to measurements have been reduced from a range of +10/-20 dB for the most recent fan noise prediction model in the NASA Aircraft Noise Prediction Program to ±3 dB or better for the proposed model in the frequency range surrounding the spectral peak. The improved relation for throttle dependence as a function of directivity is matched to measured data characteristics. Future work will pursue a framework that fits the data to relevant engine cycle parameters that may be more directly correlated with the broadband sources responsible for the throttle dependence shift at aft angles. This work has utilized a shift in spectral peak frequency relative to previous models to improve agreement with the measured data; however a general relationship between spectral peak frequency and engine characteristics has not yet

been developed. Similarly, a general directivity function has been developed based on data from two separate flight tests, although each dataset displayed some differences in directivity characteristics. Finally, future work remains to fine tune the model, develop a model for inlet-radiated broadband noise, and extend the validation of the model with an independent dataset that was not used in its development.

Despite the remaining future work, it is emphasized that the proposed model has been created using research-quality data from a highly relevant full-scale flight test on a state-of-the-art aircraft with modern engines, and has been shown to exhibit strongly improved characteristics relative to prior system-level fan noise prediction methods that were developed from model-scale fan test rig data. It is expected that the model presented in this work represents a significant improvement in the ability of NASA to predict aft-radiated fan broadband noise for both current in-service aircraft and future aircraft concepts. This will allow for better assessment of the relative performance of future aircraft concepts and noise reduction concepts that are sensitive to the relative ranking of the various noise sources on an aircraft. Better information and reduced uncertainty in noise assessments enables better investments into future technologies for maximum public benefit.

Acknowledgments

The support and funding of this research by the NASA Advanced Air Transport Technology Project is gratefully acknowledged. The Boeing Company is gratefully acknowledged for the execution of the flight tests.

References

[1] *Strategic Implementation Plan, 2023 Update*, NASA Aeronautics Research Mission Directorate, 2023.

[2] June, J. C., Thomas, R. H., and Guo, Y., "System Noise Prediction Uncertainty Quantification for a Hybrid Wing–Body Transport Concept," *AIAA Journal*, Vol. 58, No. 3, 2020, pp. 1157–1170. doi:10.2514/1.j058226.

[3] Bradley, M. K., and Droney, C. K., "Subsonic Ultra Green Aircraft Research: Phase I Final Report," NASA/CR-2011-216847, Apr. 2011. URL `https://ntrs.nasa.gov/citations/20110011321`.

[4] June, J. C., Thomas, R. H., and Guo, Y., "System Noise Technology Roadmaps for a Transonic Truss-Braced Wing and Peer Conventional Configuration," *28th AIAA/CEAS Aeroacoustics Conference*, American Institute of Aeronautics and Astronautics, 2022. doi:10.2514/6.2022-3049.

[5] Thomas, R. H., Guo, Y., Clark, I. A., and June, J. C., "Propulsion Airframe Aeroacoustics and Aircraft System Noise Flight Research Test: NASA Overview," *28th AIAA/CEAS Aeroacoustics Conference*, American Institute of Aeronautics and Astronautics, 2022. doi:10.2514/6.2022-2993.

[6] Czech, M. J., Thomas, R. H., Guo, Y., June, J. C., Clark, I. A., and Shoemaker, C. M., "Propulsion Airframe Aeroacoustics and Aircraft System Noise Flight Test on the Boeing 2020 ecoDemonstrator program," *28th AIAA/CEAS Aeroacoustics Conference*, American Institute of Aeronautics and Astronautics, 2022. doi:10.2514/6.2022-2994.

[7] Clark, I. A., Thomas, R. H., and Guo, Y., "Fan Acoustic Flight Effects on the PAA & ASN Flight Test," *28th AIAA/CEAS Aeroacoustics Conference*, American Institute of Aeronautics and Astronautics, 2022. doi:10.2514/6.2022-2996.

[8] Krejsa, E. A., and Stone, J. R., "Enhanced Fan Noise Modeling for Turbofan Engines," NASA/CR-2014-218421, Dec. 2014. URL `https://ntrs.nasa.gov/citations/20150000884`.

[9] Nesbitt, E. H., Clark, I. A., Guo, Y., and Thomas, R. H., "Flight Effects of Turbofan Fan Tones," *To be presented at the 30th AIAA/CEAS Aeroacoustics Conference*, Rome, Italy, 2024.

[10] Herkes, W. H., Olsen, R. F., and Uellenberg, S., "The Quiet Technology Demonstrator Program: Flight Validation of Airplane Noise-Reduction Concepts," *12th AIAA/CEAS Aeroacoustics Conference (27th AIAA Aeroacoustics Conference)*, American Institute of Aeronautics and Astronautics, 2006. doi:10.2514/6.2006-2720.

[11] Tukey, J. W., *Exploratory Data Analysis*, Addison-Wesley, Reading, MA, 1977.

[12] Nesbitt, E., Ganz, U., Diamond, J., and Kosanchik III, M., "An empirical prediction of inlet radiated broadband noise from full scale engines," *36th AIAA Aerospace Sciences Meeting and Exhibit*, American Institute of Aeronautics and Astronautics, 1998. doi:10.2514/6.1998-470.

[13] Kontos, K. B., Kraft, R. E., and Gliebe, P. R., "Improved NASA-ANOPP Noise Prediction Computer Code for Advanced Subsonic Propulsion Systems, Volume 2: Fan Suppression Model Development," NASA/CR-202309, Dec. 1997. URL https://ntrs.nasa.gov/citations/19970005047.

[14] Czech, M. J., and Thomas, R. H., "Open Rotor Aeroacoustic Installation Effects for Conventional and Unconventional Airframes," *19th AIAA/CEAS Aeroacoustics Conference*, Berlin, Germany, 2013. doi:10.2514/6.2013-2185.

[15] Heidmann, M. F., "Interim Prediction Method for Fan and Compressor Source Noise," Tech. Rep. TM X-71763, NASA, 1975. URL https://ntrs.nasa.gov/citations/19750017876.

[16] Hough, J. W., and Weir, D. S., "Aircraft Noise Prediction Program (ANOPP) Fan Noise Prediction for Small Engines," Tech. Rep. CR-198300, NASA, 1996.

[17] Kontos, K. B., Janardin, B. A., and Gliebe, P. R., "Improved NASA-ANOPP Noise Prediction Computer Code for Advanced Subsonic Propulsion Systems, Volume 1: ANOPP Evaluation and Fan Noise Model Improvement," Tech. Rep. CR-195480, NASA, 1996.

[18] Storn, R., and Price, K., "Differential Evolution – A Simple and Efficient Heuristic for global Optimization over Continuous Spaces," *Journal of Global Optimization*, Vol. 11, No. 4, 1997, pp. 341–359. doi:10.1023/a:1008202821328.